Mapping the protonation states of the histidine brace in an AA10 lytic polysaccharide monooxygenase using CW-EPR spectroscopy and DFT calculations†

Peter J. Lindley, [ID] Alison Parkin, [ID] Gideon J. Davies [ID] and Paul H. Walton [ID] *

The active site of the polysaccharide-degrading lytic polysaccharide monooxygenase (LPMO) enzyme features a single copper ion coordinated by a histidine brace. The primary coordination sphere of the copper contains several ligating atoms which are bonded to ionisable protons (*e.g.* OH_2, NH_2), the pK_as of which are unknown. Using a combination of CW-EPR X-band spectroscopy over a range of pH values and DFT calculations, we show that the active site of a chitin-active AA10 LPMO can exist in three different protonation states (pK_{a1} = 8.7, p$K_{a2} \sim$ 11.5), representing the ionisation of the coordinating groups. The middle pH species (fully formed at pH $\sim$ 10.5) is proposed to be $Cu(II)(His)_2(OH)_2$ (N_2O_2 coordination) with a decoordinated $R-NH_3^+$ group at the amino terminus. This species also sees a rotation of the SOMO equatorial plane from the canonical histidine brace plane, whereby the nominal Cu d($x^2 - y^2$)-orbital has rotated some 45° along the His−Cu(II)−His axis, driven by the elongation and decoordination of the amino group. The highest pH species (>12) is proposed to exist as a Cu(II)−azanide, in which the NH_2 of the amino terminus has been deprotonated. The high pH means that this species is unlikely to be biologically relevant in the catalytic cycle of AA10 LPMOs.

Introduction

Lytic polysaccharide monooxygenases (LPMOs) are copper-containing enzymes which catalyse the oxidative cleavage of glycosidic bonds within poly-saccharides.[1–3] The active site of LPMOs has been shown by crystallography to contain a single copper ion coordinated in a T-shaped configuration by a 'histidine brace', which consists of an N-terminal histidine chelating to the copper *via* its NH_2 and π−N imidazole atoms, along with the τ−N atom of a further histidine.[4]

Department of Chemistry, University of York, Heslington, York, YO10 5DD, UK. E-mail: paul.walton@york.ac.uk

In the copper(II) resting state, the structures further show that one or two exogenous ligands, usually water or hydroxide, occupy the remaining copper coordination sites.

LPMOs are divided into auxiliary activity (AA) families in the Carbohydrate Active enZyme (CAZy) database (www.cazy.org) based on sequence similarity, where so far eight distinct classes have been characterised (AA9–11, AA13–17).[1,2,5–10] The number of exogenous ligands is partly dependent on the genomic class of the LPMO. For instance, structures of AA9-classified enzymes exhibit a single water/hydroxide to give a planar N_3O coordination geometry around the copper, whereas chitin-active AA10-classified enzymes appear to show the copper(II) in a distorted square-pyramidal N_3O_2 geometry, where two exogenous water/hydroxide ligands complete the coordination sphere, as depicted in Fig. 1. In both the AA9 and AA10 cases, EPR spectroscopy has established that the SOMO is dominated by the $d(x^2 - y^2)$ orbital, requiring the ligand field of the copper to have a large sigma-bonding component in the equatorial plane of the metal ion. In the case of AA9 LPMOs, the coordination geometry of the Cu is best described as axially elongated, whereas in the case of AA10 LPMOs, EPR spectroscopy has shown *ca.* 3% of $d(z^2)$ mixing into the largely $d(x^2 - y^2)$ SOMO, commensurate with a distorted square-pyramidal geometry.[11,12]

In chitin-active AA10 LPMOs, the large number of ionisable protons of the ligands, which coordinate to the copper ion in the histidine brace (NH_2, $2 \times H_2O$), opens up the possibility that the copper(II) centre exhibits a range of different protonation states, some of which may be relevant to the enzyme's catalytic cycle. Indeed, this reasoning has extended as far as suggesting that the amino terminus can deprotonate itself to form a copper(II)–azanide bond, the σ-donating power of which is expected to be high and possibly capable of stabilising a high valent copper species.[13] Such a species may be a key intermediate in the catalytic cycle which is capable of abstracting a hydrogen atom from the polysaccharide substrate.[2,14] As such, determining the different degrees of protonation of the active site is germane to any discussion about the catalytic mechanisms of LPMOs.

It is in this context that we aimed to establish the nature of the different protonation states of the active site of an AA10 LPMO from the bacterium *Bacillus*

Fig. 1 Active site of a chitin-active AA10 LPMO, depicting the histidine brace exogenous ligands (L) ligating to the Cu(II) ion, and conserved residues.

licheniformis, *Bl*(AA10).[15] To this end, we employed CW-EPR spectroscopy in conjunction with DFT calculations to show that the active site exists in three distinct protonation states across the pH range 6.5 to 12.5. We further show that the highest pH species is most likely to be the copper(II)–azanide species proposed earlier,[2,13] but that it only exists at pH outside the usual biological range, and is not a biologically relevant species for the resting state of the enzyme.

Results and discussion

Preparation and purity of *Bacillus licheniformis* AA10 LPMO

Samples of this enzyme were prepared in *Escherichia coli* (BL21 competent cells) *via* periplasmic expression, previously reported by Courtade *et al.*[16] Crude protein was obtained from the periplasm by osmotic shock and further purified using a 5 mL HiTrap® DEAE FF anion exchanger, eluting with a NaCl gradient from 0–500 mM over 90 column volumes. LPMO-containing fractions were collected and further purified on a Superdex S75 gel filtration column (GE Life Sciences).

The purity of *Bl*(AA10) was established by gel electrophoresis, which displayed a clear and single band at *ca.* 20 kDa (ESI†). For the subsequent EPR experiments, it was important to determine that all copper in the sample was bound stoichiometrically to the active site of the enzyme. On this basis, a single equivalent of Cu was added to the enzyme from a solution of 10 mM $CuSO_4$ prior to size exclusion chromatography, from which any uncoordinated metal ions were separated from the purified enzyme.

CW-EPR X-band spectroscopy

A sample of *Bl*(AA10) (0.4 mM) was prepared in a mixed buffer system of MES, CHES, HEPES and CAPS, each at 5 mM. These buffers were chosen for their known poor-coordination properties toward metal ions and, when used synchronously, buffer a wide range of pHs. The pH of the solution was adjusted up and down by the addition of dilute solutions of NaOH and H_2SO_4, respectively. The pH of the resulting solution at room temperature was determined using a calibrated Fisherbrand™ Accumet™ AE150 Benchtop pH Meter, from which 12 samples from pH 6.5 to 12.5 were prepared in 0.5 pH unit steps. To verify that the pH extremes did not denature the protein, EPR spectra were collected on samples starting at pH 6.5 and then raising to pH 12.5, and then recollected on the same sample at a lower pH, indeed restoring the previous species.

At each pH, the sample was rapidly (<2 s) cooled[17] to 150 K and its CW-EPR X band spectrum collected.‡ The trend of the EPR spectra shows a qualitative change across the pH range, in which it is evident that all species have a spectral envelope which is consistent with a predominantly $d(x^2 - y^2)$ SOMO, showing that the Cu(II) ion at all pHs has a ligand field dominated by sigma donation in its equatorial plane (Fig. 2). Spin quantification by double integration of the spectra

---

‡ Continuous wave (CW) X-band EPR spectra were obtained using a 100 μL frozen solution of *Bl*AA10 at a concentration of 0.4 mM. Data collection was carried out on a Bruker micro EMX spectrometer using a microwave frequency of *ca.* 9.3 GHz, modulation amplitude of 4G, modulation frequency of 100 kHz and microwave power of 10.02 mW. Spectra were intensity averaged over three scans and simulated using the EasySpin 5.2.28 (ref. 27) open-source toolbox implemented by MATLAB R2020a software on a desktop PC. Raw EPR data are available at DOI: 10.15124/7a485d50-ea4e-4cd1-8fc2-650057c076af.
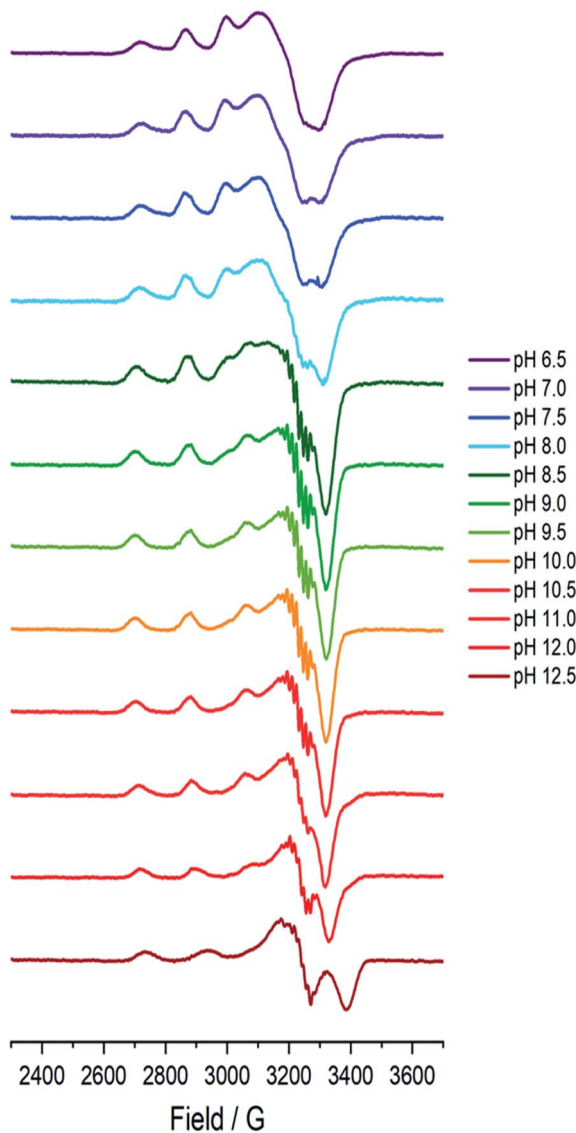
Fig. 2 Frozen solution X-band EPR spectra (150 K) of Bl(AA10) (0.4 mM) in a mixed buffer of MES, CHES, HEPES and CAPS (5 mM each) between pH 6.5 and 12.5.

also shows that there are no redox processes that occur at the active site across the pH range (ESI†).

Analysis of EPR spectra and distribution of pH dependent species

Between pHs 6.5 and 8.0, a single species is seen to dominate the spectrum, as evidenced by a single set of Cu hyperfine split peaks at low field ($g_3 = 2.260$, $A_3 = 445$ MHz). Increasing the pH leads to the formation of a new set of peaks in the low field region ($g_3 = 2.233$, $A_3 = 554$ MHz) along with distinctive superhyperfine

coupling around $g = 2.07$, commensurate with the formation of a second distinct species, the concentration of which is maximised at pH 10.5. A further increase in pH to 12.5 sees the formation of a further set of peaks in the low field region ($g_3 = 2.180$, $A_3 = 614$ MHz), consistent with the formation of a third distinct species. This final species is not fully formed at pH 12.5 but is dominant at that pH. The total number of species across the pH range was assessed using singular value decomposition analysis of the collected spectra (ESI†). From this analysis, three principal components emerged, corroborating the qualitative assessment of the pH dependence of the EPR spectra.

On the basis of the three components (species 1, 2 and 3), we sought to deconvolute the series of spectra. Given the clear separation between the different species across the pH range, it was assumed that the spectrum at pH 6.5 represented 100% of a single complex. Indeed, it was possible to simulate (with EasySpin) the lowest pH species (pH 6.5) with a single set of spin-Hamiltonian parameters (Fig. 3a and Table 1). The same was also true of the spectra collected at pH 10.5 and 12.5 (Fig. 3b and c, respectively, Table 1). In performing the simulation of species 3, we noted the appearance of a significant 'overshoot' feature which appears at high field in the species at pH 12.5. Such a feature has in the past been confused with an anomalously low g_1 value.[18]

Once spin Hamiltonian parameters of each species were obtained, it was possible to simulate the mixed species spectra (pHs 7 to 9.5 and >10.5) to determine the species distributions at each pH, from which the pK_as of species 1 (low pH) and species 2 (middle pH), and the stoichiometry of protons for each ionisation, were determined using standard methods (ESI†). The deprotonation of species 1 to 2 occurs with a pK_a of 8.7 and is a single proton step. The deprotonation of species 2 to 3 occurs with a pK_a of ~11.5 and is also a single proton step.
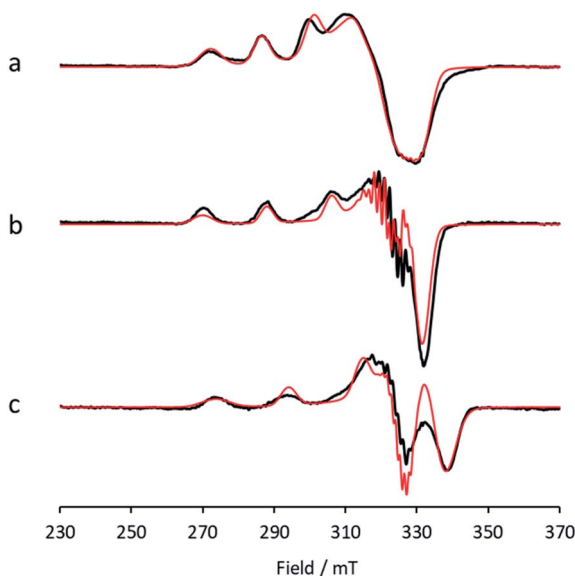

Fig. 3 X-band EPR (a) low pH species 1, with simulation (red), (b) intermediate pH species 2, with simulation (red), (c) high pH species 3, with simulation (red).

Table 1 Spin Hamiltonian parameters of the pH dependent species. It is assumed that the A_3 value is negative in sign, although this is not determined experimentally

Species	g values			Hyperfine coupling constants/MHz			
	g_1	g_2	g_3	$|A_1|$	$|A_2|$	A_3	b^2/%
1	2.030	2.125	2.260	60	90	−445	3.6
2	2.044	2.069	2.233	60	76	−554	0.8
3	2.038	2.062	2.180	70	90	−614	0.9

Ligand field analyses of spin Hamiltonian parameters

The collected spin Hamiltonian parameters of the three species are shown in Table 1. In all cases, the g values follow the pattern of $g_1 < g_2 \ll g_3$, confirming a SOMO with a high $d(x^2 - y^2)$ character. Some $d(z^2)$ mixing is evident for all species from the differences in the values of g_1 and g_2. The degree of mixing, b^2, can be calculated from the standard perturbative EPR formulae as described by Hitchman et al.,[19] which give the molecular orbital coefficients, a and b, for the SOMO defined in eqn (1) (Table 1).

$$\psi(\text{SOMO}) = a\psi(x^2 - y^2) + b\psi(z^2) \tag{1}$$

This mixing is low for species 2 and 3, revealing that the ligand field around the Cu in each of these is close to axial four-fold symmetry (note that this does not necessarily translate into a four-fold axial symmetry of the identity of the coordinating atoms, as different coordinating atoms may have similar ligand field parameters). For species 1, more mixing is evident ($b^2 = 3.6\%$), which is in-line with previous EPR studies on AA10 LPMOs[11] and the subsequent structures of these enzymes, which exhibit a distorted square pyramidal geometry around the copper ion (Fig. 1), where the exogenous ligands are two water/hydroxide molecules, one of which forms a Cu–O bond of ca. 1.9 A, and the other a more distant bond of 2.2 A.[20]

Taking the value of g_3 as a measure of the relative ligand field strengths in the equatorial plane of the copper, it is evident that this ligand field increases significantly moving from species 1 to 2 to 3, and—moreover, from the values of $d(z^2)$ mixing—that the ligand field in species 2 and 3 is relatively evenly distributed amongst the ligating atoms of the equatorial plane, suggestive of a near four-fold symmetric planar arrangement of the equatorial ligand field. Indeed, corroborating such a ligand field, the increase in A_3 value from species 1 to 2 is also known to be associated with a change in the Fermi coupling as the coordination number of the copper drops from five to four.[15] Without access to the d–d electronic transition energies, it is not possible to be more precise about the nature of the ligand field; nevertheless the trend in increasing ligand field around the equatorial plane is evident from the relative spin-Hamiltonian parameters.

Further information about the ligand field in species 2 can be obtained from the clearly delineated Cu–N superhyperfine coupling (Fig. 3b). This coupling could be accurately simulated with the inclusion of two nitrogen atoms (^{14}N, $I = 1$) in the spin Hamiltonian, in which each N atom couples to the copper with

a principal coupling value of 40 MHz. This value is similar to those already known for the Cu–His coupling constants seen in other LPMOs.[17,21] The simulation of species 2 could be adequately performed with the inclusion of two N nuclei, incommensurate with the expected N_3 coordination of the histidine brace. Additionally, the g_3 and A_3 values of species 2 place it squarely within those expected for a CuN_2O_2 coordination geometry on a canonical Peisach–Blumberg plot.[22]

In assigning a putative structure to species 2, it is informative to consider previous EPR studies on the substrate-bound state of chitin-active AA10 enzymes. These species have been well characterised as having a planar CuN_3O coordination geometry with a g_z value of 2.205 and an A_z value of ~620 MHz.[15,23] On this basis, a similar axial CuN_3O (sq. pl) ligand field is unlikely for species 2, given the discrepancies in the g_z and A_z values. This difference in the spin Hamiltonian parameters necessitates an alternative ligand field assignment for species 2. Thus, taking together the Cu spin Hamiltonian values and superhyperfine couplings, a more likely scenario is one in which the NH_2 group of the histidine brace is decoordinated from the copper (see DFT calculations below) and the coordination sphere around the Cu is made up of two histidines and two water/hydroxide ligands (see below for further discussion).

The spin Hamiltonian parameters for species 3 are distinct from those of other known LPMOs, which is particularly evident in the value of g_3 (2.18), which is lower than all known values, including the situation in which a chloride ion has entered the coordination sphere of the copper ($g_3 = 2.23$). Given the low value, we are directed towards the proposal that the ligand field around the copper in species 3 is one that is highly σ-donating, causing a large separation in the $d(x^2 - y^2)$ and $d(xy)$ orbital energies. Such a strong σ donation might be expected of a Cu–azanide interaction, which would arise from the recoordination of the $-NH_3^+$ amino terminus in species 2 which had been doubly deprotonated to give a $-NH^-$ ligating group. Commensurate with this proposal is the simulation of the superhyperfine coupling in species 3, which could only be satisfactorily achieved with the inclusion of three nitrogen atoms in the spin Hamiltonian with principal coupling constants of 35, 35 and 33 MHz (see DFT calculations below).

From the overall ligand field analysis, a hypothesis emerges for the nature of species 1, 2 and 3 and the pH-dependent ionisation processes between them. The hypothesis is depicted in Fig. 4, in which it is shown that species 2 forms via the deprotonation of a coordinating water molecule, followed by the decoordination and subsequent protonation of the $-NH_2$ group, driven by an internal proton
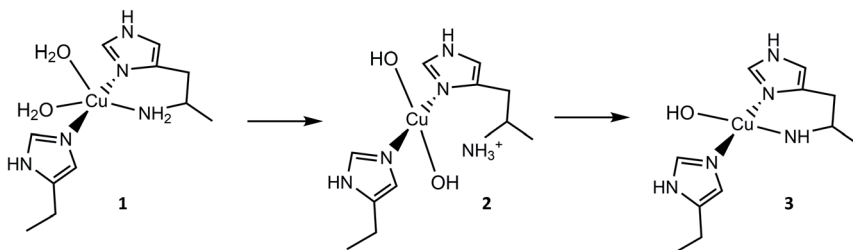

Fig. 4 Hypothetical protonation states and coordination geometries of species 1, 2 and 3.

transfer process from one of two coordinating water molecules in species 1. The formation of species 3 from species 2, on the other hand, sees the reverse proton transfer from the decoordinated $-NH_3^+$ to a coordinated hydroxide with the loss of the resulting water molecule, and the subsequent deprotonation of an N–H proton from the $-NH_2$ and recoordination to the metal as an azanide. In support of such an assignment, the formation of species 3 was accompanied by an unusual colour change from colourless to pale pink (ESI†) due to the formation of a semi-intense absorption band ($\varepsilon \approx 2500$ M^{-1} cm^{-1}) centred at 520 nm. The intensity of this band is in keeping with that of a charge transfer transition – likely arising from a ligand to metal charge transfer (LMCT) from the proposed azanide ($-NH^-$) group to the copper (see TD-DFT calculations, ESI†). Thus, the proposed ligand field changes depicted in Fig. 4 are revealed by the differences in the spin Hamiltonian parameters across the species, in which g_z decreases and A_z increases (going from species 1 to 3), commensurate with an increasing equatorial ligand field.

DFT calculations

Building on the hypothesis depicted in Fig. 4, density functional theory geometry optimisations (uBP86) and EPR calculations (uB3LYP with 38% HF exchange) were performed on the proposed species 1, 2 and 3.

In the absence of a high-resolution crystal structure for the *Bacillus licheniformis* AA10, crystallographic coordinates of the spectroscopically similar enzyme, *Bacillus amyloliquefaciens* AA10 (PDB 5IJU),[20] were used as the basis for these calculations, in keeping with the experiments of Courtade *et al.*[15] Importantly in this regard, the structure of *Ba*AA10 is one of the few LPMO structures in which the copper ion has not been photoreduced from Cu(II) to Cu(I) during the X-ray experiment.[24] Accordingly, key residues from the crystallographic coordinates were used for the basis of the calculations for species 1, retaining the primary coordination sphere and supporting residues (full information and coordinates are given in the ESI†). Following standard practice, the spatial coordinates of certain atoms at the periphery of the model were kept fixed throughout the calculation to prevent the unfettered movement of residues. These atoms are depicted in Fig. S7 (ESI†) and were selected on the basis of earlier DFT studies on a closely related LPMO.[15]

For species 1, the geometry was initially modelled with the inclusion of two ligating water molecules with bond distances based on the positioning of the oxygen atoms in the crystal structure. Notably in this regard, the water situated beneath the histidine brace plane is expected to participate in strong hydrogen bonding with a nearby aspartate residue (glutamate in *Ba*AA10), the potential of which can affect the protonation state and ligating properties of the water molecule. Indeed, upon optimisation, despite the fact that Glu and Asp residues are expected to be deprotonated across the studied pH range owing to the low pK_as of their carboxylate groups (pK_a = 2–4.5),[25] one of the protons bound to the water molecule migrated to the neighbouring carboxylate group (Fig. 5) to give a mixed hydroxide/water coordination at the Cu. Confidence in this structural assignment comes from the resulting geometry of the optimised structure, which is a close match to the crystal structure coordinates. Thus, for species 1, the coordination sphere of the Cu is best described as a distorted square-pyramid, where water and hydroxide act as exogenous ligands.
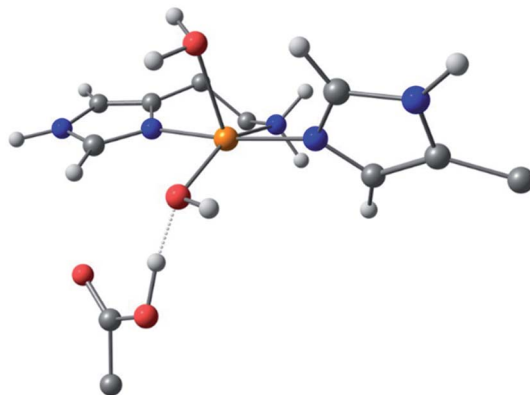
Fig. 5 DFT model of species 1 (truncated for clarity) showing the distorted square-pyramidal geometry and hydroxide/water coordination of the exogenous ligands.

While a good match was found between the optimised and experimental structures, the match between the calculated and experimental EPR parameters (Table 2) was only moderate (*e.g.* calculated $g_3 = 2.216$, experimental $g_3 = 2.26$). Moreover, the calculated Cu hyperfine values, A_1 and A_2, have relative magnitudes which are opposite to those observed experimentally. Notwithstanding the known difficulties in DFT-calculated EPR parameters matching with those from experiments, the relatively large differences seen between the experimental and calculated EPR parameters for species 1 are a recurring theme in DFT calculations on AA10 LPMO active sites in their Cu(II) resting states, even with careful selection of the basis sets and functionals.[26] As such, while the optimised structure of 1 matches well that of the experiment and is likely a good representation of the actual structure, caution must be applied in interpreting the calculated EPR data for species 1, where the reasons for the discrepancies between theoretical and experimental results remain unclear. This situation is in contrast to the calculations of the EPR parameters for species 2 and 3, which give a somewhat closer match to the experimental data (see below).

Following the ligand field analysis above, species 2 was initially modelled by removing the proton shared between the water and glutamate, and by transferring the proton attached to the second water ligand to the –NH$_2$ group (representing an overall removal of a single proton from species 1, as per the experimental

Table 2 Calculated spin Hamiltonian parameters of the pH dependent species. The *x* axis of the calculated *g* tensor lies along the His–Cu–His direction

Species	g values			Hyperfine coupling constants/MHz		
	g_x	g_y	g_z	$|A_x|$	$|A_y|$	A_z
1	2.049	2.081	2.216	110	29	−598
2	2.070	2.079	2.244	94	3	−582
3	2.037	2.070	2.188	15	140	−496

findings). Upon optimisation, the angle between the hydroxide ligands, $\angle$O–Cu–O, increased from *ca.* 90° to 157°. The divergence of the hydroxide ligands was also accompanied by the expected decoordination of the now protonated $-NH_3^+$ group from the metal and a rotation of the $d(x^2 - y^2)$ SOMO by *ca.* 45° (Fig. 6), such that the equatorial plane was now defined by the two hydroxides and the nitrogen atoms of two histidine ligands, thus completing the CuN_2O_2 coordination geometry expected from the ligand field analysis. The calculated EPR parameters (Table 2) for species 2 reflect the experimental data in that g_x and g_y are closer in values, and that the value of g_z is *ca.* 2.24.

Species 3 was modelled as a Cu(II)–azanide species formed by the expulsion of water from species 2, followed by the further removal of an $-NH_2$ proton, resulting in a short Cu–NH bond of 1.94 A (full computational details can be found in the ESI†). The optimised geometry is best described as CuN_3O planar, albeit distorted ($\angle$HN–Cu–O $\sim$160°). This distortion away from planar has been previously reported for four-coordinate LPMO structures when modelled by DFT.[15] The calculated EPR parameters for species 3 match well with those from experiments,
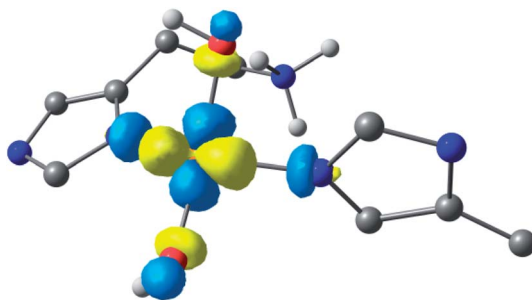

Fig. 6 Hypothetical $d(x^2 - y^2)$ dominated SOMO of species 2 showing that the orbital plane has rotated (the colours denote the orbital phases).
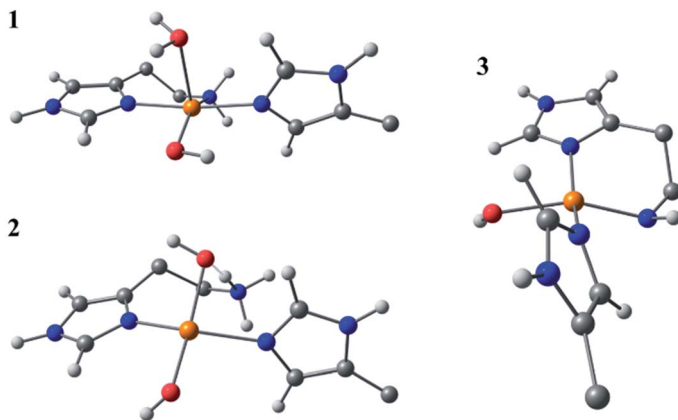

Fig. 7 DFT optimised geometries of species 1, 2 and 3. The models are truncated, and certain atoms are hidden for clarity.

most notably in the $g_{3,z}$ value of 2.18. Also, from a spectroscopic perspective, Species 3 exhibits a semi-intense UV/visible absorption band centred at 520 nm ($\varepsilon \approx 2500$ M^{-1} cm^{-1}). This band is proposed to arise from a LMCT transition from the proposed azanide group to the Cu, which is corroborated with the TD-DFT calculations (ESI†). Both the d–d and LMCT transition energies appear to be significantly blue-shifted with respect to the experimental transitions. Exact transition energies are known to carry significant error when calculated in this way for open shell systems. Nevertheless, these calculations reveal that an intense absorption band is expected for the Cu(II)–azanide complex proposed as species 3 and its energy is predicted to be positioned between the π–π* and the d–d transitions. The three optimised structures for species 1, 2 and 3 are shown in Fig. 7.

Conclusions

Herein, we establish three discrete protonation states for an AA10 LPMO within the pH range of 6.5 to 12.5, two of which are biologically relevant and may be important in the context of the LPMO mechanism. The first species exists at acidic–neutral pH and is believed to be consistent with a 5-coordinate (N_3O_2), in keeping with the current understanding of the chitin-active AA10 coordination sphere. A second species is formed by deprotonating the ligating water molecule (pK_a 8.7); yielding a near-axial EPR spectral envelope ($g_1 = 2.044$, $g_2 = 2.069$ and $g_3 = 2.233$). We hypothesise that this species exists as a N_2O_2, 4-coordinate ligand field with two hydroxide ligands and an elongated/decoordinated –R-NH$_3^+$ following proton transfer from the coordinating hydroxide to the amino terminus. This gives rise to a rotated SOMO which is no longer defined by the chelating histidine brace. The third species formed at a high pH (p$K_a \sim 11.5$) is proposed to exist as a 4-coordinate, N_3O complex, whereby species 2 has lost a water molecule (from the interaction of an OH$^-$ and NH$_3^+$) and the –NH$_2$ group has been deprotonated to form a Cu(II)–NH azanide complex. The high pH at which this species becomes accessible is outside of that which is biologically relevant and, as such, is unlikely to be pertinent in catalysis.

Conflicts of interest

There are no conflicts to declare.

Acknowledgements

Notes and references

1 G. Vaaje-Kolstad, B. Westereng, S. J. Horn, Z. Liu, H. Zhai, M. Sørlie and V. G. H. Eijsink, *Science*, 2010, **330**, 219–222.
2 R. J. Quinlan, M. D. Sweeney, L. Lo Leggio, H. Otten, J.-C. N. Poulsen, K. S. Johansen, K. B. R. M. Krogh, C. I. Jørgensen, M. Tovborg,

A. Anthonsen, T. Tryfona, C. P. Walter, P. Dupree, F. Xu, G. J. Davies and P. H. Walton, *Proc. Natl. Acad. Sci. U. S. A.*, 2011, **108**, 15079–15084.

3   C. M. Phillips, W. T. Beeson, J. H. Cate and M. A. Marletta, *ACS Chem. Biol.*, 2011, **6**, 1399–1406.

4   L. Ciano, G. J. Davies, W. B. Tolman and P. H. Walton, *Nat. Catal.*, 2018, **1**, 571–577.

5   G. R. Hemsworth, B. Henrissat, G. J. Davies and P. H. Walton, *Nat. Chem. Biol.*, 2014, **10**, 122–126.

6   V. V. Vu, W. T. Beeson, E. A. Span, E. R. Farquhar and M. A. Marletta, *Proc. Natl. Acad. Sci. U. S. A.*, 2014, **111**, 13822–13827.

7   M. Couturier, S. Ladevèze, G. Sulzenbacher, L. Ciano, M. Fanuel, C. Moreau, A. Villares, B. Cathala, F. Chaspoul, K. E. Frandsen, A. Labourel, I. Herpoël-Gimbert, S. Grisel, M. Haon, N. Lenfant, H. Rogniaux, D. Ropartz, G. J. Davies, M.-N. Rosso, P. H. Walton, B. Henrissat and J.-G. Berrin, *Nat. Chem. Biol.*, 2018, **14**, 306.

8   F. Sabbadin, G. R. Hemsworth, L. Ciano, B. Henrissat, P. Dupree, T. Tryfona, R. D. S. Marques, S. T. Sweeney, K. Besser, L. Elias, G. Pesante, Y. Li, A. A. Dowle, R. Bates, L. D. Gomez, R. Simister, G. J. Davies, P. H. Walton, N. C. Bruce and S. J. McQueen-Mason, *Nat. Commun.*, 2018, **9**, 756.

9   C. Filiatrault-Chastel, D. Navarro, M. Haon, S. Grisel, I. Herpoël-Gimbert, D. Chevret, M. Fanuel, B. Henrissat, S. Heiss-Blanquet, A. Margeot and J.-G. Berrin, *Biotechnol. Biofuels*, 2019, **12**, 55.

10 F. Sabbadin, S. Urresti, B. Henrissat, A. O. Avrova, L. R. J. Welsh, P. Lindley, M. Csukai, J. N. Squires, P. H. Walton, G. J. Davies, N. C. Bruce, S. C. Whisson and S. J. McQueen Mason, *Science*, 2021, **373**, 774–779.

11 G. R. Hemsworth, E. J. Taylor, R. Q. Kim, R. C. Gregory, S. J. Lewis, J. P. Turkenburg, A. J. Parkin, G. J. Davies and P. H. Walton, *J. Am. Chem. Soc.*, 2013, **135**, 6069–6077.

12 F. L. Aachmann, M. Sørlie, G. Skjåk-Bræk, V. G. H. Eijsink and G. Vaaje-Kolstad, *Proc. Natl. Acad. Sci. U. S. A.*, 2012, **109**, 18779–18784.

13 N. Gagnon and W. B. Tolman, *Acc. Chem. Res.*, 2015, **48**, 2126–2131.

14 J.-P. Bacik, S. Mekasha, Z. Forsberg, A. Y. Kovalevsky, G. Vaaje-Kolstad, V. G. H. Eijsink, J. C. Nix, L. Coates, M. J. Cuneo, C. J. Unkefer and J. C. H. Chen, *Biochemistry*, 2017, **56**, 2529–2532.

15 G. Courtade, L. Ciano, A. Paradisi, P. J. Lindley, Z. Forsberg, M. Sørlie, R. Wimmer, G. J. Davies, V. G. H. Eijsink, P. H. Walton and F. L. Aachmann, *Proc. Natl. Acad. Sci. U. S. A.*, 2020, **117**, 19178–19189.

16 G. Courtade, S. B. Le, G. I. Sætrom, T. Brautaset and F. L. Aachmann, *Carbohydr. Res.*, 2017, **448**, 212–219.

17 G. R. Hemsworth, L. Ciano, G. J. Davies and P. H. Walton, in *Methods Enzymol.*, ed. F. Armstrong, Academic Press, 2018, vol. 613, pp. 63–90.

18 B. Bissaro, I. Isaksen, G. Vaaje-Kolstad, V. G. H. Eijsink and Å. K. Røhr, *Biochemistry*, 2018, **57**, 1893–1906.

19 M. A. Hitchman and R. L. Belford, *Inorg. Chem.*, 1969, **8**, 958–965.

20 R. C. Gregory, G. R. Hemsworth, J. P. Turkenburg, S. J. Hart, P. H. Walton and G. J. Davies, *Dalton Trans.*, 2016, **45**, 16904–16912.

21 K. E. H. Frandsen, T. J. Simmons, P. Dupree, J.-C. N. Poulsen, G. R. Hemsworth, L. Ciano, E. M. Johnston, M. Tovborg, K. S. Johansen, P. von Freiesleben, L. Marmuse, S. Fort, S. Cottaz, H. Driguez, B. Henrissat,

N. Lenfant, F. Tuna, A. Baldansuren, G. J. Davies, L. Lo Leggio and P. H. Walton, *Nat. Chem. Biol.*, 2016, **12**, 298.

22 J. Peisach and W. E. Blumberg, *Arch. Biochem. Biophys.*, 1974, **165**, 691–708.

23 B. Bissaro, B. Streit, I. Isaksen, V. G. H. Eijsink, G. T. Beckham, J. L. DuBois and Å. K. Røhr, *Proc. Natl. Acad. Sci. U. S. A.*, 2020, **117**, 1504.

24 A. Paradisi, M. J. Steward, P. Lindley, G. J. Davies and P. H. Walton, in *Reference Module in Chemistry, Molecular Sciences and Chemical Engineering*, Elsevier, 2020, DOI: 10.1016/B978-0-12-409547-2.14928-5.

25 M. J. Harms, C. A. Castañeda, J. L. Schlessman, G. R. Sue, D. G. Isom, B. R. Cannon and B. E. García-Moreno, *J. Mol. Biol.*, 2009, **389**, 34–47.

26 Y. A. Theibich, S. P. A. Sauer, L. L. Leggio and E. D. Hedegård, *Comput. Struct. Biotechnol. J.*, 2021, **19**, 555–567.

27 S. Stoll and A. Schweiger, *J. Magn. Reson.*, 2006, **178**, 42–55.